RNA modifications on Adenosine Regulate Macrophage Function

Valerie Griesche[†], Salvatore Di Giorgio[†], Julia Brettschneider, Irem Tellioglu, Chih-Yuan Kao, Jose Paulo Lorenzo , Laura Pezzella, Georg Stoecklin, F. Nina Papavasiliou*.*

[1] Division of Immune Diversity, German Cancer Research Center, Heidelberg 69120, Germany.
[2] Graduate program of Faculty of Biosciences, Heidelberg University, Heidelberg 69120, Germany.
[3] Mannheim Institute for Innate Immunoscience (MI3), Medical Faculty, Heidelberg University, Mannheim, Germany
[4] Division of Cancer Epigenomics, German Cancer Research Center, Heidelberg 69120, Germany.
[5] Department of Statistics, Mathematical Sciences. University of Warwick, Coventry, UK

[†] Contributed independently

*Correspondence: salvatore.digiorgio@dkfz.de, n.papavasiliou@dkfz.de

Abstract

Macrophages are important innate immune cells that respond rapidly to inflammatory cues and fulfill diverse functions in the activation, execution and resolution of immune and inflammatory responses. Currently, there is no comprehensive understanding of the combinatorial effect of mRNA modifications in a single cell type, the consequences for mRNA processing and metabolism, and how these changes affect cell physiology. We use the mouse macrophage line RAW264.7 (RAW) to systematically address the combinatorial effect of two major mRNA modifications during macrophage stimulation: adenosine to inosine deamination (A-to-I), and adenosine N6 methylation (m6A). At the functional level we found that both METTL3 (the m6A writer) and ADAR1 (the adenosine deaminase) are

required for full activation of RAW macrophages (as determined by expression of surface markers) and for optimal phagocytosis (a key macrophage function). Using both short read and single molecule sequencing on RAW cells with genetic deletions of the m6A writer METTL3 and the A deaminase ADAR1, we found that loss of m6A affected A-to-I levels while m6A levels remained relatively stable. A detailed investigation of potential interactions between m6A and A-to-I at the single transcript level is ongoing.

Introduction

Dynamic mRNA modifications have a crucial impact on the fate and metabolism of a transcript including splicing, subcellular localization, stability and translation[1]. N6-methyladenosine (m6A) and A-to-I editing are among the most prominent modifications found in mRNA. The reversible methylation of adenosine (A) is catalyzed by the Methyltransferase 3 (METTL3) which forms part of the m^6A writer complex and preferably modifies the consensus PuPuACX (Pu = purine; X = A, C, or U) motif. M6A is enriched after the last splice site of the last exon and in the 3' untranslated region (3'UTR) in proximity to the stop codon [1,2]. The functions of m6A include regulation of transcript stability, translation efficiency and splicing based on subcellular localization of the transcript and association with distinct m6A readers[3–9]. Recent studies identified m6As role in preventing formation of double stranded RNA (dsRNA) structures and their recognition by innate immune sensors[10] .

Similar to METTL3, adenosine deaminases acting on RNA-1 (ADAR1) also modify adenosine bases. Two different ADAR1 isoforms exist, constitutively expressed nuclear p110 and interferon-induced cytoplasmic p150 important in stress and anti-viral responses. ADAR family members recognize dsRNA and deaminate A to Inosine (I) which is decoded as Guanosine[11]. Thereby, breaking the dsRNA structure and preventing activation of innate immune sensing pathways[12]. Additional roles of ADAR1-mediated RNA editing include recording events and alterations of splice sites. A-to-I editing occurs most frequently in repetitive elements such as short interspersed nuclear elements (SINE), introns, and the 3'UTR, due to their propensity to form dsRNA structures [11].

Both m6A and A-to-I RNA editing target adenosine, potentially acting within overlapping regions and interacting with one another. While several studies have investigated their relationship, many questions regarding their interplay remain unresolved. In breast cancer, ADAR1 increases *METTL3* transcript as well as m6A levels in an editing dependent manner. Mechanistically, A-to-I editing of *METTL3* mRNA alters a miRNA binding site, leading to increased METTL3 expression[11]. In glioblastoma METTL3 directly methylates *ADAR1*

mRNA. Methylation of *ADAR1* mRNA leads to its association with m6A reader YTHDF1 promoting translation into protein[13]. Globally, A-to-I RNA editing and m6A negatively correlate, as seen in reduced ADAR1 association and RNA editing in methylated transcripts and increased A-to-I editing upon METTL3 deletion on respective m6A depleted transcripts. Interestingly, studies have also identified a subset of methylated transcripts which showed increased A-to-I editing levels as compared to their unmethylated transcript, yet this subset of transcripts was not further examined [14].

Macrophages are phagocytic innate immune cells found in all tissues of mammals. In response to changes in tissue physiology and external stimuli, macrophages can readily adapt their phenotype and function. The distinct macrophage phenotypes have been classified in proinflammatory, classically activated M1-like macrophages and anti-inflammatory, alternatively activated M2-like macrophages. However, macrophages do not persist in a strictly defined fixed state, but dynamically change their phenotype in the wide range of pro- and anti-inflammatory states underlining their plasticity[15]. Previous research has highlighted the diverse roles of RNA modifications in immune cell development, differentiation, activation, migration, and polarization, thereby shaping the immunological response[16]. In macrophages, m^6A was reported to positively regulate M1 polarization by stabilization of *STAT1* mRNA and to prime macrophages to increase phagocytosis capacities[17]. METTL3 was also shown to regulate macrophages' inflammatory response through NF-κB signaling possibly by *TRAF6* mRNA methylation [18,19] and the M6A reader IGF2BP2 has been reported to regulate macrophage activation by preventing TSC1 and PPARγ degradation[20]. Similarly, ADAR1 has been reported to function in promoting macrophage activation through NF-κB signaling[21], and lack of ADAR1 was shown to inhibit NF-κB signaling and downstream inflammation mediators (like inducible nitric oxide synthase (iNOS) and IL-1β[22 25]).

Thus, it is clear that m6A and A-to-I deamination independently function in the regulation of macrophage activity.

Here we study the dynamics and relationship of m6A and A-to-I RNA editing in resting macrophages and their changes during proinflammatory stimulation. Using Nanopore Direct RNA sequencing, Illumina sequencing and functional assays, we aim to decipher interdependencies between these two modifications and their impact on macrophage function.

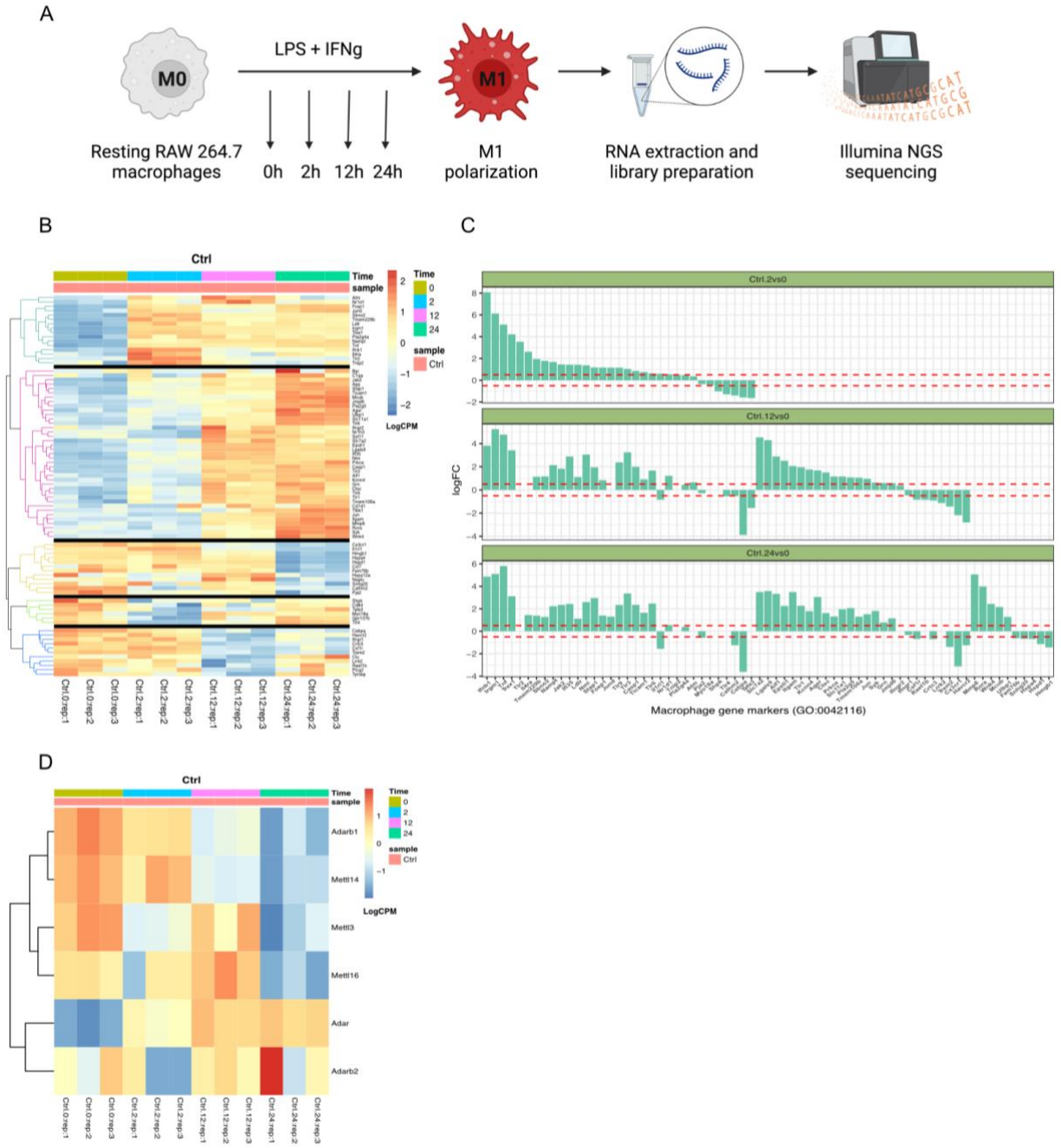

Figure 1. (A) Schematic representation of polarization assay. (B) Heatmap of macrophage markers gene expression (GO:0042116). The heatmap illustrates the expression dynamics of macrophage marker genes during LPS-IFNγ treatment over a time course of control samples. Expression values are presented as LogCPM, with rows representing individual genes and columns representing sample replicates at different time points. Hierarchical clustering of genes was performed using Euclidean distance of gene expression profiles, and the resulting dendrogram is displayed on the left. **(C) LogFC of significantly differentially expressed macrophage marker genes.** Genes were selected based on statistical significance (FDR < 0.05). The bar plot shows the log2FC values for these genes, arranged in descending order of magnitude (left to right). Gene identifiers are displayed on the x-axis. **(D) Heatmap of Deaminases and Methyltransferase expression.** The heatmap displays the expression levels of enzymes responsible for RNA modifications, specifically A-to-I and m6A, in Ctrl samples under untreated and LPS-IFNγ-treated conditions. Expression values are presented as LogCPM.

A

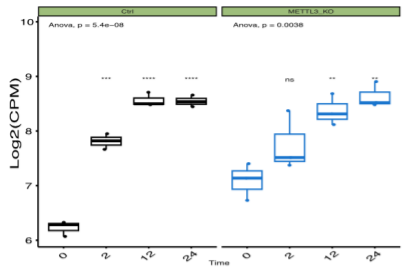
Ctrl
METTL3_KO
Anova, p = 5.4e−08
Anova, p = 0.0038
Log2(CPM)
Time

B

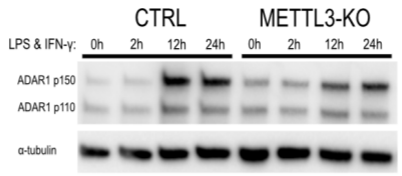
CTRL
METTL3-KO
LPS & IFN-γ: 0h 2h 12h 24h 0h 2h 12h 24h
ADAR1 p150
ADAR1 p110
α-tubulin

C

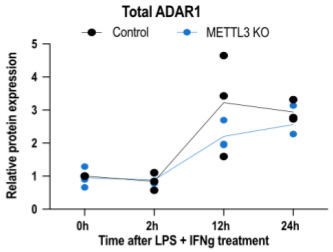
Total ADAR1
Control
METTL3 KO
Relative protein expression
Time after LPS + IFNg treatment

D

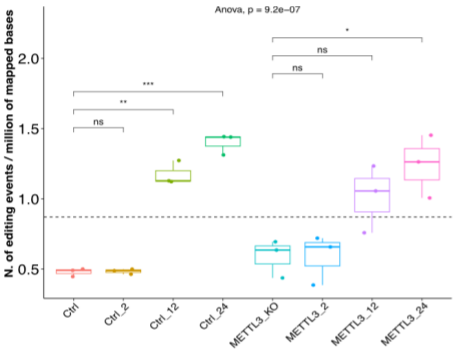
Anova, p = 9.2e−07
N. of editing events / million of mapped bases
Ctrl
Ctrl_2
Ctrl_12
Ctrl_24
METTL3_KO
METTL3_2
METTL3_12
METTL3_24

G

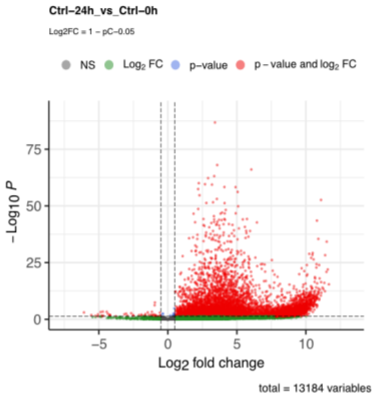
Ctrl−24h_vs_Ctrl−0h
Log2FC = 1 – pC−0.05
NS
Log2 FC
p−value
p – value and log2 FC
−Log10 P
Log2 fold change
total = 13184 variables

H

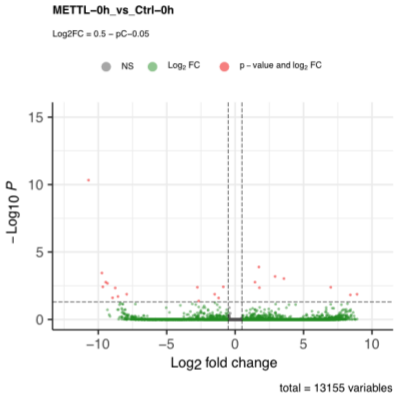
METTL−0h_vs_Ctrl−0h
Log2FC = 0.5 – pC−0.05
NS
Log2 FC
p – value and log2 FC
−Log10 P
Log2 fold change
total = 13155 variables

I

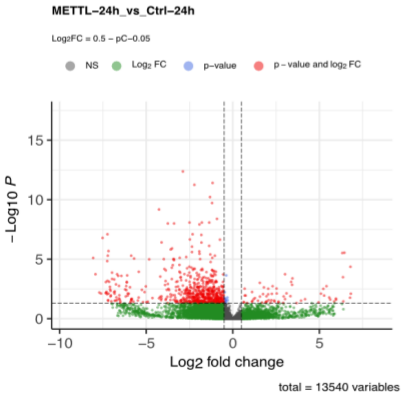
METTL−24h_vs_Ctrl−24h
Log2FC = 0.5 – pC−0.05
NS
Log2 FC
p−value
p – value and log2 FC
−Log10 P
Log2 fold change
total = 13540 variables

Figure 2. (A) Boxplots illustrating the expression levels of Adar mRNA across various LPS-IFNγ treatment time points (0, 2, 12, and 24 hours) in Control (Ctrl) and METTL3 Knockout (KO) conditions. Statistical analysis was performed using a global ANOVA test, with pairwise comparisons conducted through post hoc t-tests. Significance levels are denoted as follows: $*p < 0.05$; $**p < 0.01$; $***p < 0.001$; $****p < 0.0001$. **(B)** Representative Western blot of ADAR1 protein expression during the time course of stimulation. **(C)** Quantification of total ADAR1 protein levels. **(D)** Boxplots representing the number of editing events (with coverage ≥ 30) normalized by millions of mapped bases. **(E)** Differential editing sites identified in Control (Ctrl) samples after 24 hours of LPS-IFNγ treatment compared to untreated Ctrl samples. **(F)** Differential editing sites in untreated METTL3-KO compared to untreated Ctrl. **(G)** Differential editing sites (DES) in METTL3-KO compared to Ctrl after 24 hours of LPS-IFNγ treatment. In panels **(E–G)**, vertical dashed lines represent a log2FC of -0.05 and 0.05, while horizontal dashed lines indicate a p-value threshold of 0.05.

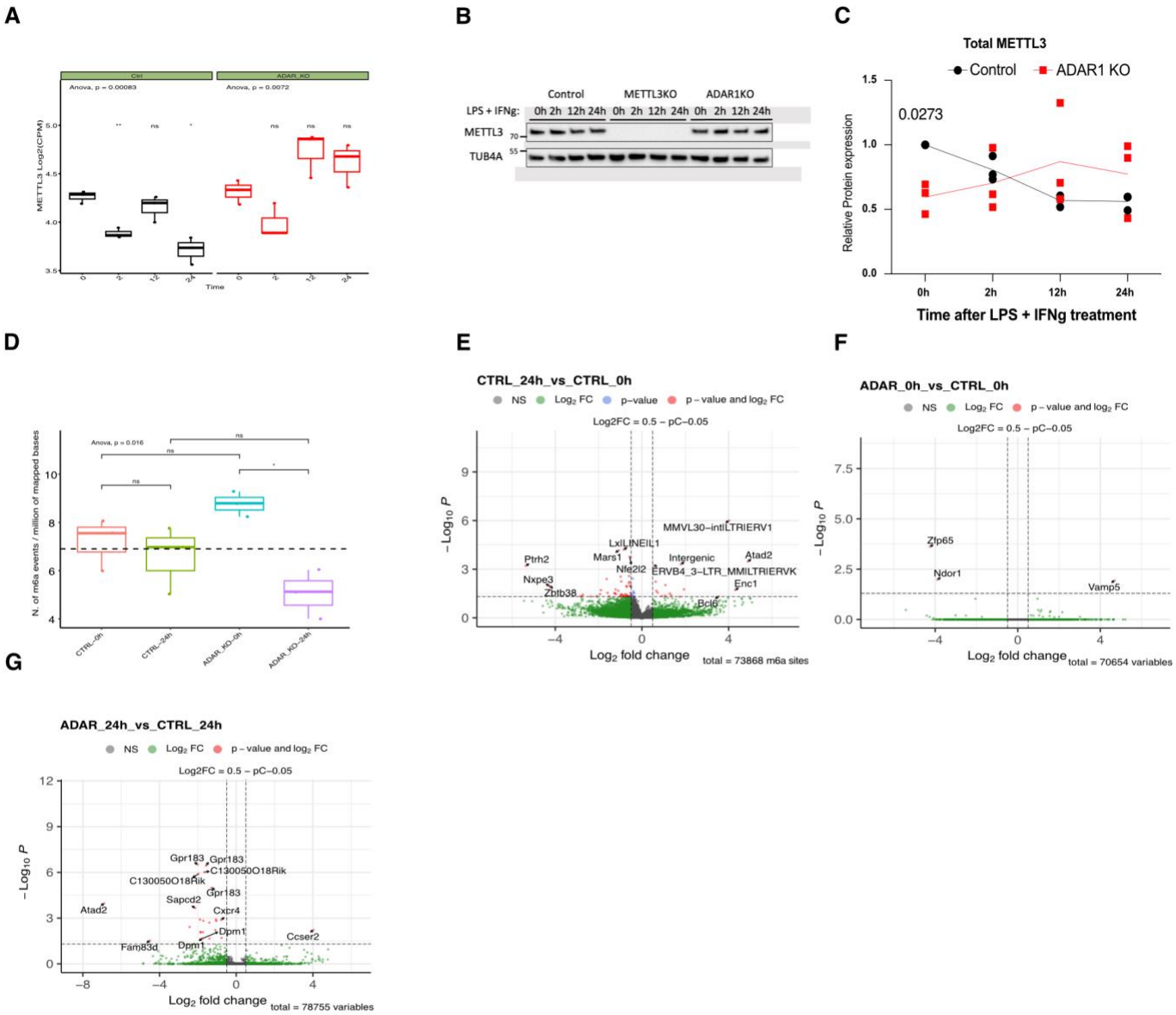

Figure 3. (A) Boxplots illustrating the expression levels of METTL3 mRNA across various LPS-IFNγ treatment time points (0, 2, 12, and 24 hours) in Control (Ctrl) and ADAR Knockout (KO) conditions. Statistical analysis was performed using a global ANOVA test, with pairwise comparisons conducted through post hoc t-tests. Significance levels are denoted as follows: $*p < 0.05$; $**p < 0.01$; $***p < 0.001$; $****p < 0.0001$. (**B)** Representative Western blot of METTL3 protein

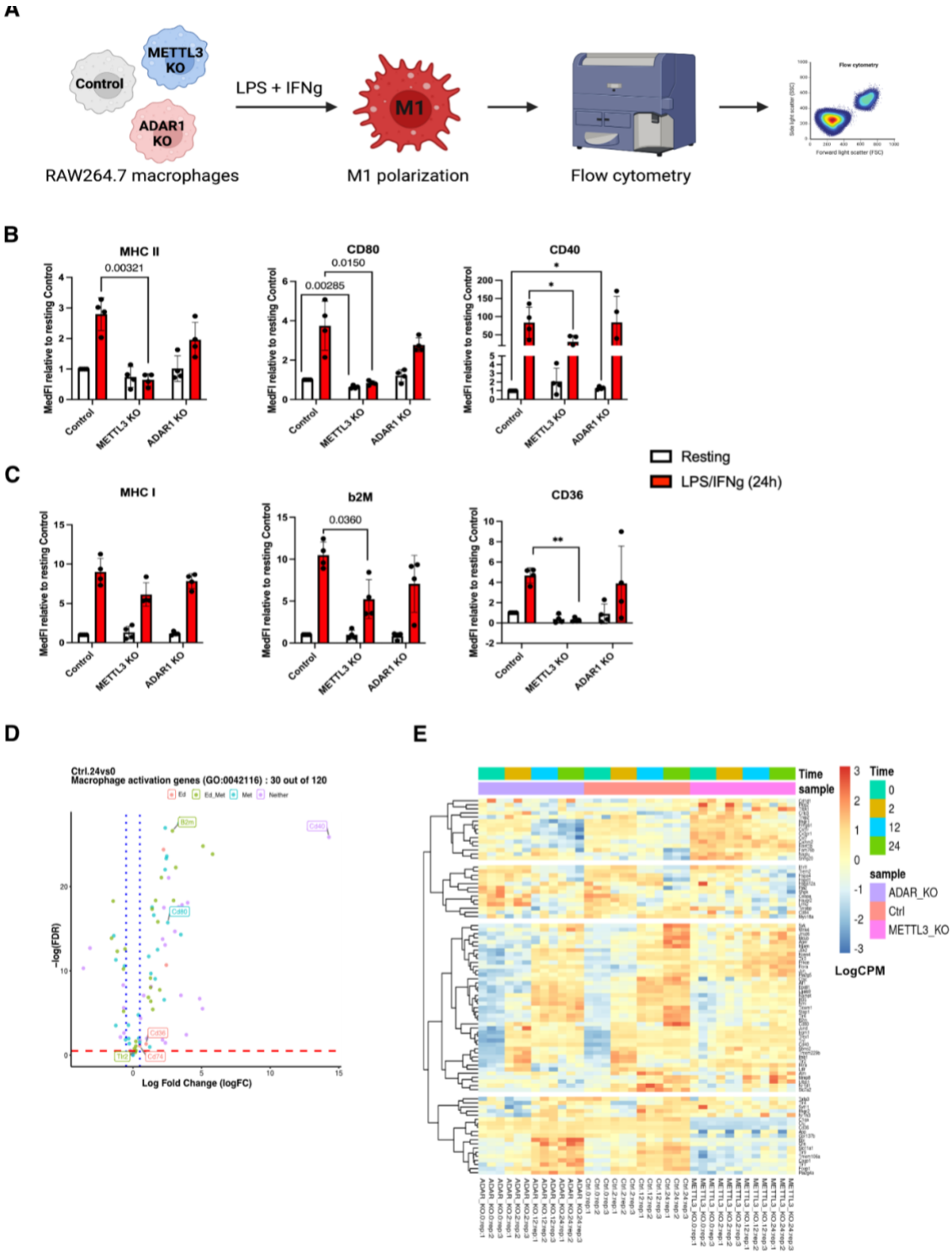
A
Control
METTL3 KO
ADAR1 KO
RAW264.7 macrophages
LPS + IFNg
M1
M1 polarization
Flow cytometry
B
MHC II
CD80
CD40
MedFI relative to resting Control
Control
METTL3 KO
ADAR1 KO
Resting
LPS/IFNg (24h)
C
MHC I
b2M
CD36
D
Ctrl.24vs0
Macrophage activation genes (GO:0042116) : 30 out of 120
-log(FDR)
Log Fold Change (logFC)
E
Time
sample
ADAR_KO
Ctrl
METTL3_KO
LogCPM

Figure 4: Changes in cell surface marker expression in METTL3 KO and ADAR1 KO macrophages. A) Schematic representation of workflow. **B)** Analysis of activation associated cell surface markers by flow cytometry at rest and 24h after LPS and IFNg treatment. p values ≤ 0.1 based on paired two-tailed t test are indicated. **D)** Volcano plot illustrating differentially expressed macrophage activation markers (GO:0042116) in Control (Ctrl) samples at 24 hours post-LPS-IFNγ treatment, compared with untreated Ctrl samples. Genes are color-coded according to the presence of RNA editing and/or methylation: red for edited genes, green for genes that are both edited and methylated, light blue for genes with one or more

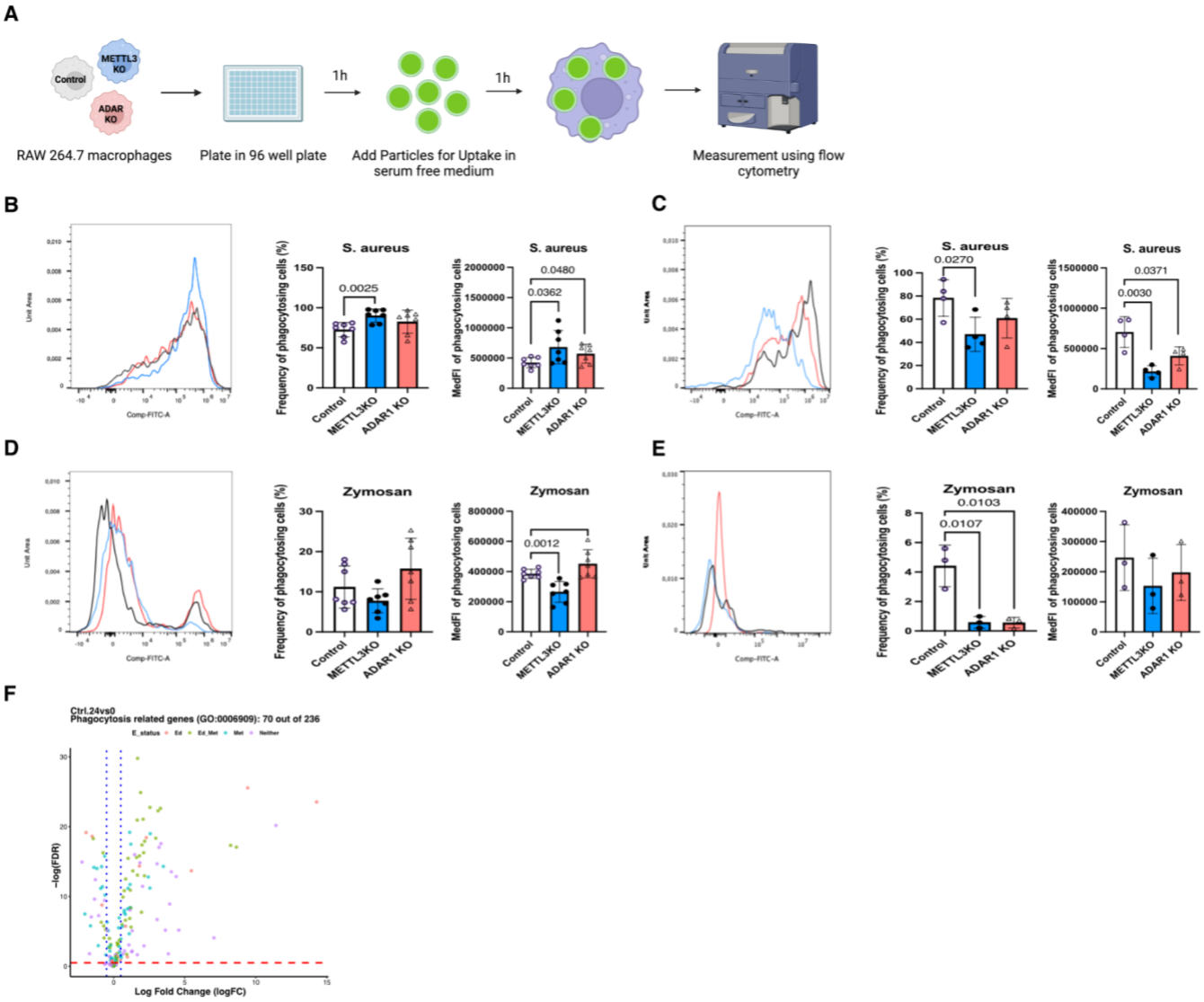

Figure 5. **Impact of Adenosine mRNA modifications on Phagocytosis**. **A)** Schematic representation of phagocytosis assay. **(B-E)** Phagocytosis by non-stimulated Control, METTL3 KO and ADAR1 KO macrophages of *S. aureus* **(B)** and Zymonsan **(C)**. **(D-F)** Phagocytosis by Control, METTL3 KO and ADAR1 KO macrophages pre-stimulated for 24h with LPS and IFNg of *S. aureus* **(D)** and Zymonsan **(E)**. **F)** Volcano plot illustrating differentially expressed phagocytosis related genes (GO:0006909) in Control (Ctrl) samples at 24 hours post-

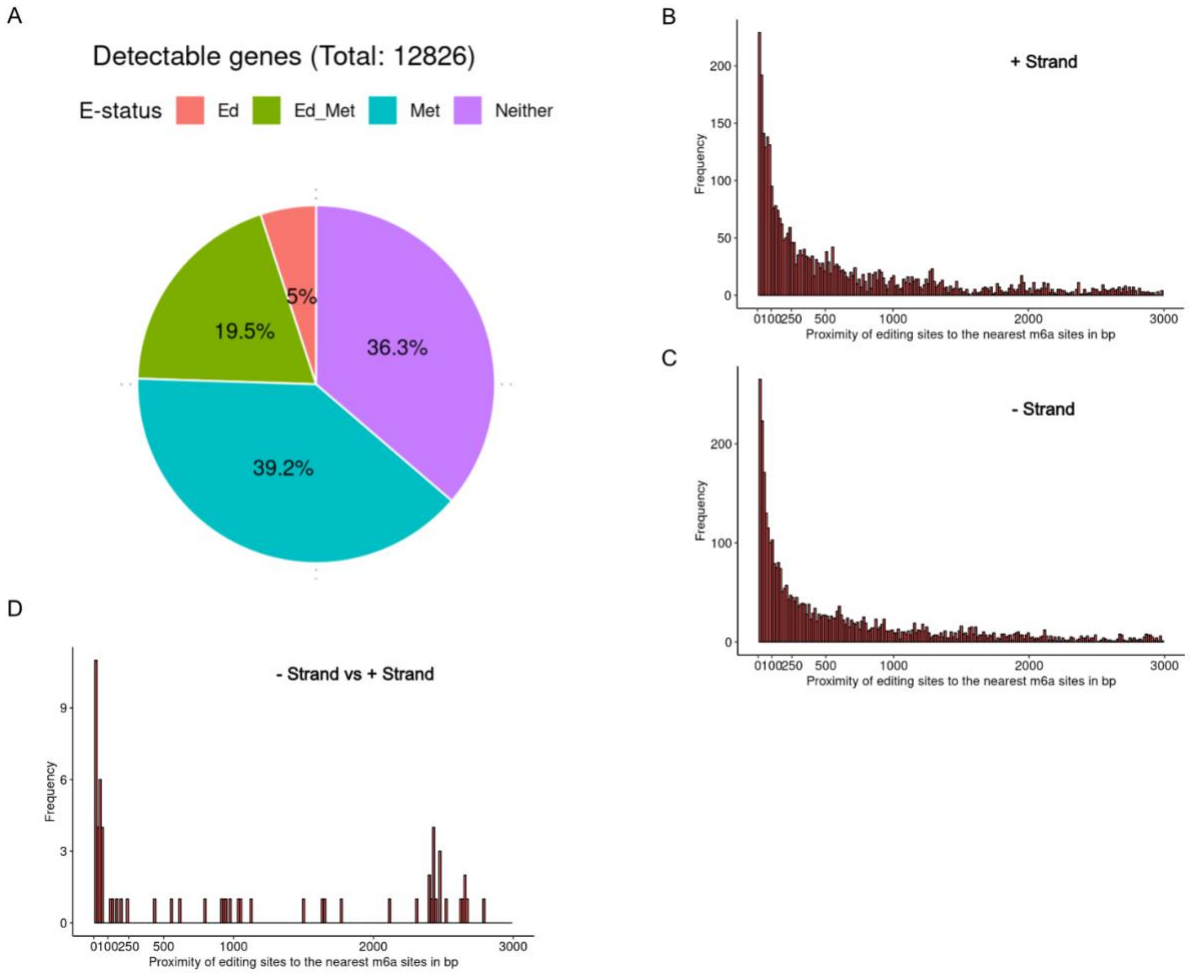

Figure 6: Distrbiution of modification sites over expressed genes and their distance over the gene body.

(A) Pie chart showing all detectable genes, classified based on the presence of A-to-I editing site, m6A modification site, both, or neither.

(B–D) Distributions of distances between the nearest m6A and A-to-I sites on the plus, minus, or opposite

Results

The response of naive RAW 264.7 macrophages to proinflammatory stimulation by combined LPS and IFN-y treatment. Both A-to-I and m6A tend to overlap in their distribution along the gene body, as both modifications commonly occur near transcript termination sites (TTS) and within the 3′UTR [2,23–25]. This proximity suggests a potential interplay between the two types of adenosine modifications. To investigate their dynamics and possible functional relationship during macrophage activation, we focused on the RAW264.7 macrophage cell line. Proinflammatory stimulation of RAW264.7 macrophages elicits rapid transcriptional changes characteristic of macrophage activation (GO:0042116), with key genes upregulated as early as 2 hours post-stimulation (**Fig. 1B**). Distinct temporal response expression patterns emerged, underscoring the dynamic nature of this response. Genes such as Tnf, Ifnb1, Tlr2, and Trex1, which are typically expressed at low levels under basal conditions, showed a marked increase in expression beginning at 2 hours. In contrast, genes with negligible basal expression—Tlr1, Jun, Tlr6, Tlr3, Tlr9 exhibited robust induction at 12 hours. Meanwhile, genes that are constitutively expressed in macrophages demonstrated phased downregulation at various stages after stimulation, as Il1rl1, Tlr4, Cahlm2, Cebpa, Cx3cr1 and Trem2. These temporal patterns are more clearly illustrated in the bar plot of log fold-change (LogFC), ordered by expression magnitude and progressing from 2 to 24 hours (top to bottom) (**Fig. 1C**). Finally, it is notable that both ADAR1 and METTL3 are present in these cells during stimulation with ADAR1 levels increasing with IFN treatment (as expected) while METLL3 levels remaining relatively stable (dropping only at the 24h timepoint) (**Fig.1D**)

Loss of METTL3 from RAW 264.7 macrophages affects A-to-I editing levels. To assess potential interactions between m6A and adenosine deamination we generated clonal cell lines lacking either the A-to-I editing enzyme ADAR1 or the catalytic subunit of the m6A writer complex METTL3. (**Sup. Fig. 1 and 2**). At the outset of this study, A-to-I detection was not yet feasible with nanopore sequencing. Therefore, we opted to use the well-established Illumina sequencing platform to investigate ADAR1 expression and the associated RNA editing during macrophage activation, as well as to examine how these processes are influenced by the absence of METTL3 As the ADAR1 p150 isoform is interferon inducible, we expected increased levels of ADAR1 expression upon LPS and IFN-y treatment. Indeed, both control and METTL3-KO samples exhibited an upregulation of Adar1 mRNA beginning at 2 hours post-stimulation, which continued to increase at later time points (**Fig. 2A**). No significant differences in Adar1 expression were observed between the two groups. Protein levels followed a similar trend, albeit with a delay, as increases in ADAR1 protein were detectable only at 12 and 24 hours post-stimulation (**Fig. 2B–C**).

On the other hand, we investigated whether RNA editing sites exhibited differential editing or changes in their global number between conditions. Upon inflammatory stimulation, the number of editing sites increased in parallel with protein levels, peaking at 24 hours (**Fig. 2D**). Additionally, many editing sites exhibited increased editing levels starting from 12 hours (data not shown) in the control (Ctrl) condition and progressing 24 hours (**Fig. 2E**). The mean editing levels at these sites increased significantly, rising from approximately 10% in the steady state to around 30% after stimulation (**Sup. Fig. 2**). Both effects highlight a clear editing response to inflammation.A similar effect was observed in the METTL3-KO condition regarding the editing number, although editing levels in treated METTL3-KO samples were slightly lower compared to Ctrl (**Sup. Fig. 2**).

Differential editing analysis between METTL3-KO and Ctrl in the steady state revealed that only 6 genes exhibited higher editing levels in Ctrl, while 11 genes displayed reduced editing levels. (**Fig. 2F**, **Sup. Table 1**). However, the situation changed 24 hours post-treatment, with many editing sites showing reduced editing levels in the METTL3-KO condition (**Fig. 2G**). This reduction could potentially reflect an interaction between the two modifications, as some of these genes were found to have editing sites positioned close to m6A deposition sites. Alternatively, it could indicate a reduced availability of regions for editing in METTL3-KO, which remains to be investigated.

Loss of ADAR1 from RAW 264.7 macrophages does not interfere with m6A levels. Next, we focused on clones lacking the A-to-I editing enzyme ADAR1 to examine how its loss might affect METTL3 expression and m6A deposition. Mettl3 mRNA levels remained widely unaffected by proinflammatory stimulation in Control as well as ADAR1 KO cells (Fig. 3A). While unstimulated Control cells expressed slightly more METTL3 protein as compared to ADAR1 KO, this difference was no longer observed during macrophage activation which was characterized by largely stable METTL3 protein expression independent of ADAR1 expression (Fig. 3B-C).

We employed nanopore direct RNA sequencing to investigate the status of m6A modifications. Given that the most significant increases in RNA editing and major changes in gene expression were identified after 24 hours, we sequenced samples only at their steady states and 24 hours post-stimulation. The global number of m6A sites (including those outside the canonical DRACH motif) appeared unaffected by inflammatory stimulation in the Ctrl condition. However, a reduction in m6A sites number was observed in ADAR-KO samples 24 hours after stimulation compared to their corresponding controls (**Fig. 3D**). We further investigated whether m6A frequency per site was affected by the stimulus in the Ctrl condition and, surprisingly, found that global m6A levels remained unaffected by the inflammatory response in this cell line (**Fig. 3E**). Only a few sites were differentially methylated (**Sup. Table 2**). Consistently, m6A sites exhibit nearly identical methylation levels between Ctrl and ADAR-KO samples, as well as between their respective treated conditions (**Fig. 3F-G**), with only a few exceptions (**Sup. Table 2**).

Impact of adenosine modifications on macrophage activation. After identifying global changes in m6A and A-to-I upon proinflammatory stimulation, we focused on the impact of the mRNA modifications on macrophage function. We observed RNA editing events and m6A sites in several transcripts associated with macrophage activation raising the question if they play a direct role in macrophage activation **(Fig. 4D)**. As described above, upon LPS and IFN-y treatment macrophages transcriptionally upregulated a variety of activation makers and inflammatory cytokines, many of which showed changes in absence of ADAR1 or METTL3 (**Fig. 4E**). Control macrophages displayed increased cell surface expression of activation markers typically associated with M1 polarization, including MHC II, CD80, CD40, and β2M (required for MHC I presentation). While ADAR1 KO macrophages closely mimicked the controls, METTL3 KO macrophages showed a strong deficiency in upregulation of all of these surface markers, most pronounced for MHC II and CD80 (**Fig. 4B**). Notably, all of these molecules play an important role in antigen presentation and co-stimulation of a T cell response, hence, facilitating the communication between macrophages and the adaptive immune system. Also M1 marker and scavenger receptor CD36 failed to be upregulated in METTL3 KO macrophages during pro-inflammatory

stimulation (**Fig. 4C**). Interestingly, when investigating expression of TLR2, which is involved in recognizing different pathogen associated molecular patterns (PAMPs) and phagocytosis, we observed increased expression in resting METTL3 KO cells as compared to control or ADAR1 KOs, while equal expression levels were observed in control and both KOs after pro-inflammatory stimulation (**data not shown**).

Impact of adenosine modifications on phagocytosis. As we observed changes in surface receptor expression which mediate the key macrophage function of phagocytosis, we asked if phagocytosis activity was affected by loss of ADAR1 or METTL3. We identified many phagocytosis related genes upregulated upon LPS and IFN-y treatment, which contained m6A, A-to-I editing sites or both **(Fig. 5F)**. To functionally test if the RNA modifications impacted phagocytosis, resting macrophages were incubated either with *S. aureus* or the yeast cell wall component zymosan in an assay where these particles would emit fluorescent signals only when they would reach the acidic environment of an endosome (thus allowing quantification by FACS analysis). While an equal number of control and ADAR1 KO cells phagocytosed *S. aureus*, ADAR1 KO cells took up slightly higher amounts of bacteria per phagocytosing cell. Unstimulated METTL3 KO cells showed a pronounced increase in both the percentage of cells taking up *S. aureus* and in numbers of particles taken up per cell (**Fig. 5B**). In contrast, the cells' capacity to take up zymosan was decreased in the absence of METTL3 while it was not affected by ADAR1 (**Fig. 5C**).

As we previously observed impaired activation of METTL3 KO macrophages after proinflammatory stimulation, we wanted to test if this was accompanied by attenuated phagocytosis activity. Hence, we repeated the phagocytosis assay with macrophages pre-stimulated for 24 h with LPS and IFN-y. Interestingly, pre-stimulated METTL3KO and ADAR1KO cells took up significantly lower amounts of *S. aureus* per cell as compared to pre-stimulated controls (**Fig. 5D**). Also the uptake of zymosan was strongly reduced in both KOs as compared to controls (**Fig. 5E**). Together, these findings indicate that phagocytosis is affected by loss of either METTL3 or ADAR1 but also that these modifiers phagocytosis differentially (likely reflecting the differences in receptors and pathways affected). Further, the role of RNA modifiers on phagocytosis capacities change between resting and pre-stimulated macrophages.

Interdependencies between m6A and A-to-I modifications. To begin to assess an interplay, if any, between the two adenosine modifications, we first assessed how prevalent they were across the transcriptome. Among the approximately 12,000 detectable genes, more than half contained at least one modification site. Specifically, 5% of these genes exhibited only A-to-I editing sites, 19.5% had both m6A and A-to-I sites, and 39.2% displayed only m6A sites. Only 36% of genes are apparently free of modification (**Fig. 6A**).

Although METTL3 and ADAR1 are thought to target different substrates—METTL3 acting on single-stranded RNA (often on canonical DRACH motifs) and ADAR1 on double-stranded RNA (dsRNA)—their interaction remains possible. At the time of this analysis, Nanopore models capable of detecting A-to-I editing were not yet available. As an alternative, we measured the distance between A-to-I sites and the closest m6A sites. Surprisingly, we identified ~460 genes containing ~700 modification sites located within 50 bp of each other. Of these, 169 genes harbored 267 modification sites separated by less than 10 bp (**Fig. 6B-C**). This proximity was only observed when both modifications were located on the same strand. When measuring the distance

between modifications on opposite strands, no such proximity was detected (**Fig. 6D**). The exact nature of these potential interactions is the focus of our current work.

Discussion

Macrophage cells exemplify remarkable plasticity. These cells must respond to a diverse array of stimuli to maintain tissue homeostasis and defend against a multitude of threats. Achieving this requires highly orchestrated, well-regulated, and rapid responses that extend beyond direct transcriptional and translational changes, incorporating modulation of the epitranscriptome and the dynamic modification of RNA molecules. This additional layer of regulation enables a faster and more adaptive response, shaping macrophage behavior and guiding these cells into specific activation states. These activation states are not confined to the extremes of M1 (pro-inflammatory) and M2 (anti-inflammatory) polarization, but instead represent a continuum of specialized functions tailored to meet specific environmental and physiological demands. This versatility equips macrophages to perform their roles with precision and efficiency, underscoring their importance in immune regulation and tissue repair.

The proinflammatory stimulus represented by LPS and IFN-γ treatment mimics an M1 activation response - and as we and others have shown, this response is temporally dynamic: it is characterized by the early induction of genes such as Ifnb1 and Tnf (among many other LPS-responsive genes) that are rapidly activated through the promotion of transcription elongation from a poised transcription initiation complex, ensuring a rapid onset of the response [23,24]. These genes then orchestrate the activation of intermediate and late response genes [25], many of which are modified (Supplementary Fig. 4).

As expected, Adar deaminase activity increases after stimulation, accompanied by a global increase in the number of editing sites, which follows the rise in protein levels in both Ctrl and METTL3-KO samples, with no significant differences observed between the two conditions. Another measure of editing activity, the global frequency of editing events per site, is strongly induced by IFN-γ, as shown in Fig. 2E. In the steady state, no differential editing is observed between Ctrl and METTL3-KO samples. However, upon stimulation, many editing sites, belonging to approximately 300 genes, exhibit lower editing levels in METTL3-KO compared to the control. These results suggest a potential negative impact of m6A absence on A-to-I editing frequencies, indicating that in the absence of m6A, ADAR may edit less efficiently. This observation aligns with previous findings, which reported a positive link between m6A and RNA editing, although this relationship appears to depend more on the m6A reader YTHDF1 upregulation rather than solely on m6A itself. This mechanism seems to play a role in inhibiting the feedback loop and preventing excessive activation of interferon (IFN) responses.[47]

This evidence should be considered preliminary: at the time of the initial analysis, the nanopore base-calling model was only capable of detecting m6A sites. This limitation made it impossible to determine whether m6A and A-to-I modifications co-occur within the same transcript, hindering the ability to further investigate their relationship. Consequently, this prevents either confirming or refuting previous reports suggesting that methylated transcripts exhibit reduced editing levels [14]. It is plausible that multiple subsets of transcripts coexist, with some exhibiting a negative interaction between m6A and A-to-I modifications, while others display a positive relationship. This duality could be further supported by the fact that the effects of m6A are mediated

not only directly but also through a network of cofactors, adding an additional layer of complexity to this regulatory mechanism.

Material and Methods

Cell culture

RAW264.7 cells were cultured in cell-culture treated vessels in DMEM (high glucose) supplemented with 10 % FCS, 1 % L-glutamine, and 1 % penicillin/streptomycin at 37 °C, 5 % CO_2, and relative humidity 90 %. For M1 polarization, cells were stimulated with 100 ng/ml LPS and 20 ng/ml IFN-y for indicated durations.

Generation of RAW 264.7 knockout and control cell lines

Guides targeting the genomic sequence of METTL3 (exon 1: GCGAGAGATTGCAGCGGCGA, exon 3: GGGCGGCAAATTTCTGGAGA), and Adar1 (exon 2: ACTCTAACAACCCGCTGACA), as well as non-targeting control guides (GCTTTCACGGAGGTTCGACG, ATGTTGCAGTTCGGCTCGAT) were cloned into plasmid pSpCas9(BB)-2A-GFP (PX458, Addgene, #48138, a gift from Feng Zhang). RAW 264.7 cells were nucleofected with plasmids using Amaxa's Cell Line Nucleofector Kit V (Lonza, 10507935) and the manufacturer's protocol for Nucleofector II Device. 48 h after nucleofection, cells were resuspended in cell sorting buffer (PBS supplemented with 2 % FCS, 25 mM HEPES, and 2mM EDTA), stained with Propidium iodide (Invitrogen, BMS500PI) for live/dead discrimination and GFP expressing clones were single-cell sorted for ADAR1 and METTL3 KO clones and sorted in bulk for the non-targeted control using the BD Aria 3 Cell Sorter.

Validation of KO cell lines

After expansion, clonal cell lines were screened for biallelic indels by amplification of the targeted gene region by polymerase chain reaction (PCR) using Q5 high-fidelity DNA polymerase (NEB, M0491L) with associated reagents according to NEB's standard protocol and Sanger Sequencing. Knockouts were confirmed on the protein level using Western blot. For METTL3 KO clones, transcript isoforms regulated by m6A mRNA modification were quantified by reverse-transcription quantitative PCR (RT-qPCR) as described below.

Flow cytometric analysis of cell surface markers

Unstimulated or cells stimulated for 24h with 100 ng/ml LPS and 20 ug/ml IFNg were harvested in FACS buffer (PBS supplemented with 2 % FCS), incubated for 10 minutes in homemade Fc blocking buffer, stained for 30 minutes with antibody staining cocktail in FACS buffer, followed by 30 min staining with violet live/dead fixable staining solution (Invitrogen, 34964, 1:1000 in PBS), and fixation for 10 minutes with 4 % Paraformaldehyde (Thermo, 28908) in PBS. Between steps, cells were washed by adding an excess FACS buffer and centrifugation for 5 minutes at 800 g at 4°C. Samples were analyzed using the BD Canto II flow cytometer. Antibodies used: CD40 APC/fire, Biolegend, 124632; CD36 APC, Biolegend, 102611; I-A/I-E FITC, Biolegend, 107605; APC anti-mouse β2-microglobulin, Biolegend, 154505; H-2 PE, Biolegend, 125505; CD80 PE, BD, 553769).

Phagocytosis assay

For unstimulated samples, 100 000 cells were plated in flat-bottom 96-well plates in fresh medium and allowed to attach for 1 h. For stimulated samples, 10 000 cells were plated two days before phagocytosis assay and treated for 24h with 100 ng/ml LPS and 20 ug/ml IFNg. Cells were washed twice with non-supplemented DMEM (high glucose), followed by adding 5 ug pHrodo Green S. aureus (Invitrogen, P35367) or Zymosan (Invitrogen, P35365) in 50 ul non-supplemented DMEM. Cells were incubated with particles for uptake for 1 h at 37°C. Cells were harvested, incubated for 30 minutes with violet live/dead fixable staining solution (1:1000 in PBS), and washed. Cells were analyzed at the BD Cytek Aurora Spectral Flow Cytometer using automated spectral unmixing.

Next Generation Sequencing (NGS)

For NGS sequencing, RNA extraction was performed using the RNeasy Mini kit (Qiagen, 74104) according to the manufacturer. Contaminating DNA was removed using the Turbo DNase-free Kit (Invitrogen, AM1907) according to the manufacturer. RNA was quantified by Nanodrop and submitted to the DKFZ Core Facility for library preparation (rRNA depletion protocol) and sequenced using NovaSeq 6000 Sequencing System (Illumina).

Direct RNA sequencing using Oxford Nanopore Technology

Unstimulated and cells treated for 24 h with LPS and IFN-y treatment were lysed in Trizol and RNA was extracted using Zymo Direct-Zol Kit (Zymo, R2050) including DNase I treatment. Libraries were prepared from 2.5 µg total RNA using the Direct RNA Sequencing Kit (SQK-RNA004) according to the manufacturer. Libraries were loaded on the PromethION RNA Flow Cell (FLO-PRO004RA) on the promethION 24 sequencing device.

RNA LC-MS/MS

Unstimulated and cells treated for 24 h with LPS and IFN-y treatment were lysed in Trizol and RNA was extracted using Zymo Direct-Zol Kit (Zymo, R2050) including DNase I treatment. Poly-A enrichment was performed using the NEBNext Poly(A) mRNA Magnetic Isolation Module (NEB). RNA samples from three replicates were pooled and RNA was precipitated overnight at -70°C using ammonium acetate (Sigma, A2706) and ice-cold ethanol. RNA was digested and internal standards of ^{13}C labeled yeast RNA was added. Calibration samples of unmodified and modified nucleotides were prepared. Samples were injected into the LC-MS/MS instrument for measurement. Data was analyzed using the Aligent Masshunter qualitative and quantitative software.

Reverse transcription (RT) and RT qPCR

RNA extraction for downstream reverse transcription was performed using the RNeasy Mini kit (Qiagen, 74104) according to the manufacturer. Contaminating DNA was removed using the Turbo DNase-freeKit

(Invitrogen, AM1907) according to the manufacturer. Reverse transcription was performed using ProtoScript First Strand cDNA Synthesis Kit (NEB, E6300L) with random primers according to the manufacturer. Quantitative PCR, was performed using iTaq Universal SYBR Green Supermix (Biorad, 1725121) according to the manufacturer using the CFX Connect Real-Time System (Bio-Rad). Samples were normalized by the amount of the housekeeper CPH (CPH_fw: ATGGTCAACCCCACCGTG ; CPH_rv: TTCTTGCTGTCTTTGGAACTTTGTC) present in each sample.

Western blot

Cultured cells were washed with PBS and lysed in Cell Lysis Buffer (Cell signaling, 9803) containing cOmplete, Mini, EDTA-free Protease Inhibitor Cocktail (Roche, 11836170001) and 1 mM phenylmethylsulfonylfluoride (Sigma, 93482, 1:100) for 30 minutes on ice, followed by centrifugation for 15 min at 10 000 g at 4 °C. The protein in the supernatant was quantified using the Pierce BCA Protein Assay Kit (Thermo, 23225) according to the manufacturer, and was cooked with Laemmli buffer for 5 minutes at 95 °C. Samples were loaded on Mini-PROTEAN TGX Precast Gels (4-15%, Bio-Rad, 4561086) and run for 30 minutes at 70 V followed by 130 V until reaching desired separation. Proteins were transferred to a Nitrocellulose Blotting Membrane (Cytiva) using a wet blotting system for 70 minutes at 100 V. The nitrocellulose membrane was blocked for 1 h with 5 % skim milk in TBS-T (1X TBS with 0.1 % Tween-20). Membranes were incubated with primary antibodies (METTL3, Abcam, ab195352; ADAR 1, Santa cruz, sc-73408, beta-actin, Sigma, A5441; alpha Tubulin, Abcam, ab4074) in 5 % milk - TBS-T overnight at 4 °C while rotating. Membranes were washed three times with TBS-T and incubated with corresponding horseradish peroxidase-coupled secondary antibodies (goat anti mouse - HRP (H+L), Biorad, 170-6516; goat anti rabbit-HRP (H+L), Biorad, 170-6515) in 5 % skim milk - TBS-T for 1 h at room temperature while shaking. After three washes with TBS-T, membranes were incubated with chemiluminescence based detection reagent 1 and 2 at equal volumes (ECL Start Western Blotting Detection Reagent, Cytiva, RPN3243, or SuperSignal West Pico PLUS Chemiluminescent Substrate, Thermo, 34095). Chemiluminescent signals were detected using the ChemiDoc Imaging System (BioRad). Densiometric quantification was performed using the ImageG software. Amount of protein was normalized against the amount of the housekeeper control in each sample.

Illumina RNA-seq data processing

Adapters were trimmed using trimmomatic v0.38 1 [48] with follow command line:

```
“trimmomatic.sh PE -threads 15 /${S_name}_R1.fastq.gz /${S_name}_R2.fastq.gz
/Trimmed/${S_name}_R1_paired.fastq.gz /Trimmed/${S_name}_R1_unpaired.fastq.gz
/Trimmed/${S_name}_R2_paired.fastq.gz /Trimmed/${S_name}_R2_unpaired.fastq.gz ILLUMINACLIP:/Illumina.fa:3:30:7
MINLEN:50”
```

Alignment of fastq files to the GRCm38 genome was performed using STAR 2 v.2.5.3.a [49] and the parameters detailed below.

```
“STAR --runMode alignReads --readFilesCommand zcat --genomeDir /UCSC_GRCm38/STAR_index_2.5.3a --readFilesIn
${S_name}R1_paired.fastq.gz ${S_name}_R2_paired.fastq.gz --outFileNamePrefix ${S_name} --runThreadN 10 --
outFilterMultimapNmax 1 --outSAMstrandField intronMotif --outSAMtype BAM SortedByCoordinate”
```

Bams quality was checked using qualimap v2.2.
Output bam files were sorted and indexed using samtools v1.5[50].

Illumina RNA-editing calling and processing

RNA editing candidates were identified using REDItools[51] v2.0, employing the reditools.py script with the following parameters:

```
“reditools.py -f ${S_name}_Aligned.sortedByCoord.out.sorted.dedup.bam -o
/REDITOOLED/${S_name}_Aligned.sorted_reditooled.txt -s 2 -T 2 -os 4 -m
/REDITOOLED/homopol/${S_name}_Aligned.sorted_homopol.txt -c
/REDITOOLED/homopol/${S_name}_Aligned.sorted_homopol.txt -r /UCSC_GRCm38/mm10.fa -sf
/UCSC_GRCm38/Splicesites/mm10_splicesites.ss -q 25 -bq 35 -mbp 10 -Mbp 10”
```

Key parameter settings included a minimum read mapping quality of 25 (-q 25), a minimum base quality of 35 (-bq 35), and exclusion of the first and last 10 bases of each read (-mbp 10 -Mbp 10).
Additional parameters specified were: strand-specific mode 2 (-s 2), strand confidence mode 2 (-T 2), and a minimum homopolymer length of 4 (-os 4).

The output files generated by Reditool were processed using a custom in-house script (**1.Make_reditoolbackground.R**). This script is designed to identify genomic regions that consistently exhibit no edits in the context of A-to-G transitions, representing A-to-I editing as detected by Illumina sequencing (Ctrl_Positions). The script executes the following steps:

- **Filtering:** ADAR-KO Reditool output files are processed to discard sites with more than one substitution type. Only genomic positions with a minimum coverage of 10 reads and no substitutions reported (indicated by the AllSubs column = "-") are retained.
- **Replicate and Sample Type Selection:** Genomic positions are required to be present in at least 2 out of 3 biological replicates and in at least 2 out of 4 sample conditions, ensuring a consistency threshold of 50%.
- **Aggregation:** The script aggregates genomic positions by genomic region and sample type. For each site, the median values of read coverage and the frequency of the alternative allele (expected to approximate 0) are calculated.

These steps are designed to ensure the reliability and consistency of RNA editing calls across the studied samples, enhancing subsequent filtering of false positives and SNPs.

In the next step, the in-house script “2.0.0.RNA_editing_Filtering.R” utilizes the previously generated list of genomic positions (Ctrl_Positions) to identify overlapping sites in CTRL and METTL3-KO samples that exhibit A-to-G mutations, indicative of A-to-I editing as detected by Illumina sequencing. The filtering criteria for retaining candidate editing events involve two main stages:

1. Raw Editing Sites Database Creation.

This step aims at reducing the file size and optimizing subsequent steps for faster processing. The criteria applied during this stage are as follows:

- **Filtering Covered Positions:** Genomic positions (Ctrl_Positions) are filtered to keep only those with a median coverage of ≥10 across sample replicates.
- **Ctrl Positions Matching:** Positions are cross-referenced with the previous filtered Ctrl_Positions, and only matching sites are retained.
- **Filtering Editing Candidates**: Genomic positions with multiple substitution types are discarded, while positions exhibiting A-to-G substitutions and a coverage of ≥5 are retained.

2. Refining Candidate Edited Positions.

- **Replicate and Sample Group Consistency:** Candidate edited positions must be present in at least 2 out of 3 biological replicates and in at least 2 out of 8 sample group conditions.
- **Coverage:** Candidate edited positions with a median coverage of ≥10 within sample replicates are kept.
- **Editing Frequency Support:** Candidate edited positions are further filtered based on the median count of read supporting the editing site of ≥5 across sample replicates.

The script produces three output files, each tailored for specific analyses in this study:

2.Editing_sites_db_Gt10_Al5_Mc10.txt.gz: This file contains a list of edited sites filtered according to the criteria outlined above. It will be referred to as **DB1** in this study.

2.Editing_complete_db_Gt10_Al5_Mc5.rds: This database includes a comprehensive list of genomic positions with editing observed in some samples (DB1). It highlights the presence of unedited positions overlapping with edited sites. This file is used for analyses requiring all positions, such as differential editing analysis, and will be referred to as **DB2** in this study.

2.Editing_baseline_db_Gt10.rds: This file contains editing candidates with a coverage of ≥5. It is particularly useful for adjusting other filtering criteria, such as estimating consistency across sample groups or calculating global editing site counts and editing frequencies. This file will be referred to as **DB3** in this study.

Editing sites effect prediction and Annotation

The impact of editing sites was analyzed using the Ensembl Variant Effect Predictor (VEP)[52]**,** integrated into an in-house R script executed via the command line.

Editing sites per sample quantification

The number of mapped bases for each sample was obtained using Samtools[50] stats. This value was then used to normalize the corresponding number of editing sites per sample. The normalization formula applied is as follows:

$$\boldsymbol{Normalized\ Editing\ Sites} = \frac{\boldsymbol{Number\ of\ Editing\ Sites}}{\frac{\boldsymbol{Mapped\ Bases}}{\boldsymbol{10^6}}}$$

This normalization ensures that the number of editing sites is scaled relative to sequencing depth, enabling more reliable comparisons between samples.

DB3 was used to count the number of editing sites, applying the following filtering criteria: editing sites present in at least 2 out of 3 biological replicates, a median total coverage of ≥10, and a median number of reads supporting editing sites of ≥5. All positions with an editing frequency ≠ 0 were then included in the count.

This filtering approach undoubtedly increases the potential inclusion of low-quality editing sites or false positives. However, assuming the error rate remains consistent across all samples, any observed differences between samples should primarily reflect true differences in editing sites, even if of lower quality.

Differentially Edited sites detection

Differential editing sites (DES) were identified using the DSS[53] R package, implemented in an in-house script "**7.0.Differential_RNA_Editing_DSS.R**" with the smoothing option disabled. Originally developed for differential methylation (DM) detection, DSS employs a rigorous Wald test for beta-binomial distributions. The test statistics account for both biological variations (characterized by the dispersion parameter) and sequencing depth. Candidate editing sites from **DB2** were used as input for this analysis. The log2 fold change (log2FC) was calculated using the following formula:

$$Log2FC = log2(\mu_1 + 1) - log2(\mu_2 + 1)$$

Gene expression analysis

The quantification was performed using Salmon v0.14.2[54] in mapping-based mode, providing an efficient and accurate method for transcript quantification. The following command line was used to execute Salmon:

```
"salmon quant --numBootstraps 20 -i /UCSC_GRCm38/SALMON_index/ -l A -1
/Trimmed/${Sample_name}_R1_paired.fastq.gz -2
/Trimmed/${Sample_name}_R2_paired.fastq.gz -p 25 -o
/SALMON_expr/${Sample_name} --validateMappings"
```

The Salmon outputs were imported into EdgeR[55] via the tximport[56] package, which produces gene-level estimated counts and an associated edgeR offset matrix. Differential analysis for gene counts was performed using the EdgeR[55], implemented in an in-house code. Significantly upregulated/downregulated genes were determined by abs(logFC)>0.5 and FDR < 0.05. The volcano plot was generated using the EnhancedVolcano R package[57].

Nanopore direct-RNAseq preprocessing

The pod5 files were basecalled using the ONT basecaller Dorado v0.7.0, with the models "rna004_130bps_hac@v5.0.0" and "rna004_130bps_hac@v5.0.0_m6A@v1" for the kit "SQK-RNA004".

Basecalling was performed on a GPU (Tesla V100-SXM2-32GB) to ensure high-performance processing. The command line used is as follows:

```
“dorado basecaller --min-qscore 6 --emit-moves hac,m6A /ont/raw/i0039410/data/1184237/pod5_pass/ --reference /UCSC_GRCm38/mm10.fa --mm2-preset splice:uf:k14 > /ONT/Bams_dorado_Genome/File.bam”
```

--hac,m6A: Specifies the models used for basecalling. The hac model (rna004_130bps_hac@v5.0.0) is the high-accuracy model for standard basecalling, while the m6A model (rna004_130bps_hac@v5.0.0_m6A@v1) is used for detecting m6A RNA modifications. At the time of the initial analysis, the detection of inosine modifications was not available as an option in the modification detection settings.

--mm2-preset splice:uf:k14: Configures the minimap2 alignment preset for mapping RNA reads, optimized for spliced alignment.

Output bam files were sorted and indexed using samtools[50] v1.5.

Nanopore m6a detection

The BAM files were processed to generate modification BED files using Modkit v0.3.1. For m6A calling, the parameters --filter-threshold A:0.8 and --mod-threshold m:0.99 were applied, as determined by the modification probability density plot and HeatMap generated using Modkit sample-probs output files (Supplementary Fig3 A-B).

Modkit sample-porbs command line:

```
“modkit sample-probs -t 20 --percentiles 0.1,0.5,0.95 -f 0.3 --hist --only-mapped --force --prefix ${S_name} -o /m6a_Res/${S_name}.bam”
```

Modkit pileup command line:

```
“modkit pileup -t 20 --log-filepath /m6a_Res/Pileup/${S_name}.log --sampling-frac 0.4 --max-depth 20000 --with-header --filter-threshold A:0.8 --mod-thresholds a:0.99 ${S_name}.bam /m6a_Res/Pileup/${S_name}.bed”
```

M6a preprocessing

Modkit sample-probs results revealed no discernible differences in m6A counts between METTL3-KO and control samples when using threshold values below 0.99 (**Supplementary Fig. 3A–B**). This finding suggests a high likelihood of false-positive m6A sites at lower thresholds or, less plausibly, residual methylation mediated by other methyltransferases.

To discover potential m6A sites, we began by identifying differentially methylated (DM) candidates under the assumption that changes in methylation frequency highlight bona fide m6A modifications dependent on METTL3. We then performed two separate comparisons using METTL3-KO (untreated and LPS-IFNγ 24 h) as the negative control. Specifically, we compared:

1. **ADAR** (untreated and LPS-IFNγ 24 h) **versus** METTL3-KO (untreated and LPS-IFNγ 24 h).
2. **CTRL** (untreated and LPS 24 h) **versus** METTL3-KO (untreated and LPS-IFNγ 24 h).

These comparisons allowed us to pinpoint potential DM sites that differ between ADAR or CTRL samples and METTL3-KO under corresponding conditions (**Supplementary Fig3 C-G**).
These comparisons employed the R package DSS[53] within an in-house script, with the smoothing option disabled. While smoothing is designed for CpG island analyses, where m6A sites often exhibit strong spatial correlations, it can produce false positives in RNA data by labeling m6a site flanking regions as m6A-positive despite zero actual m6a read count.

For the DM analysis, genomic positions were initially filtered as follows:

1. **Coverage Threshold:** Only positions with a coverage of ≥10 reads across samples were retained.
2. **Replicate and Sample Group Consistency:** Candidate edited positions must be present in at least 2 out of 3 biological replicates, and in both sample groups being compared.

Eliminating positions that showed no change between target and METTL3-KO samples yielded a final set of m6A candidate sites, including their genomic coordinates, coverage data, and log2 fold-change relative to the corresponding knockout samples. At this stage, no filtering was applied based on the number of modified reads supporting a methylated position or logFC; these thresholds will be established later, according to the specific requirements of downstream analyses.

In a second step, the m6A candidate sites identified in the previous comparisons were merged to generate a comprehensive list of potential m6A sites. This list was then used to retrieve corresponding positions from the BED methylation files (for ADAR-KO and CTRL samples), producing a consolidated dataset of potential m6A positions observed in 2 or more samples. Notably, this approach also incorporates unmethylated positions overlapping putative m6A sites. The sites used for list building were filtered with a criterion of $|Log2FC| \leq 0.5$ and $FDR < 0.05$. Any additional filtering of these methylated positions was performed based on the specific requirements of subsequent analyses.

M6a sites per sample quantification

For this analysis, m6A sites were selected based on criteria requiring a minimum total coverage of 10 reads and at least 5 reads supporting the m6A site. Although total coverage and the number of supporting reads may not always be sufficient to reliably distinguish true m6A sites from false positives, the error rate is expected to be consistent across the entire library of samples. Consequently, any observed changes, if present, should be attributed to genuine m6A sites. The number of m6A sites was then normalized using the same approach previously applied to editing sites.

M6a Annotation

m6A sites were annotated and profiled across gene body regions using [58] and Homer[59].

Data Availability

The data for this study will be made available once the manuscript has been conditionally accepted.

References

1. Shi, H., Chai, P., Jia, R. & Fan, X. Novel insight into the regulatory roles of diverse RNA modifications: Re-defining the bridge between transcription and translation. *Mol. Cancer* **19**, 78 (2020).
2. Meyer, K. D. *et al.* Comprehensive Analysis of mRNA Methylation Reveals Enrichment in 3′ UTRs and near Stop Codons. *Cell* **149**, 1635–1646 (2012).
3. Meyer, K. D. *et al.* 5′ UTR m6A Promotes Cap-Independent Translation. *Cell* **163**, 999–1010 (2015).
4. Zhou, J. *et al.* Dynamic m6A mRNA methylation directs translational control of heat shock response. *Nature* **526**, 591–594 (2015).
5. Wang, X. *et al.* N6-methyladenosine Modulates Messenger RNA Translation Efficiency. *Cell* **161**, 1388–1399 (2015).
6. Xiao, Z. *et al.* METTL3-mediated m6A methylation orchestrates mRNA stability and dsRNA contents to equilibrate γδ T1 and γδ T17 cells. *Cell Rep.* **42**, (2023).
7. Zhao, X. *et al.* FTO-dependent demethylation of N6-methyladenosine regulates mRNA splicing and is required for adipogenesis. *Cell Res.* **24**, 1403–1419 (2014).
8. Wang, X. *et al.* N6-methyladenosine-dependent regulation of messenger RNA stability. *Nature* **505**, 117–120 (2014).

9. Huang, H. *et al.* Recognition of RNA N6-methyladenosine by IGF2BP Proteins Enhances mRNA Stability and Translation. *Nat. Cell Biol.* **20**, 285–295 (2018).

10. Gao, Y. *et al.* m6A Modification Prevents Formation of Endogenous Double-Stranded RNAs and Deleterious Innate Immune Responses during Hematopoietic Development. *Immunity* **52**, 1007-1021.e8 (2020).

11. Wulff, B.-E. & Nishikura, K. Substitutional A-to-I RNA editing. *Wiley Interdiscip. Rev. RNA* **1**, 90–101 (2010).

12. Mannion, N. M. *et al.* The RNA-Editing Enzyme ADAR1 Controls Innate Immune Responses to RNA. *Cell Rep.* **9**, 1482–1494 (2014).

13. Tassinari, V. *et al.* ADAR1 is a new target of METTL3 and plays a pro-oncogenic role in glioblastoma by an editing-independent mechanism. *Genome Biol.* **22**, 51 (2021).

14. Xiang, J.-F. *et al.* N6-Methyladenosines Modulate A-to-I RNA Editing. *Mol. Cell* **69**, 126-135.e6 (2018).

15. Wynn, T. A., Chawla, A. & Pollard, J. W. Origins and Hallmarks of Macrophages: Development, Homeostasis, and Disease. *Nature* **496**, 445–455 (2013).

16. Cui, L. *et al.* RNA modifications: importance in immune cell biology and related diseases. *Signal Transduct. Target. Ther.* **7**, 1–26 (2022).

17. Liu, Y. *et al.* The N6-methyladenosine (m6A)-forming enzyme METTL3 facilitates M1 macrophage polarization through the methylation of STAT1 mRNA. *Am. J. Physiol.-Cell Physiol.* **317**, C762–C775 (2019).

18. Wang, J., Yan, S., Lu, H., Wang, S. & Xu, D. METTL3 Attenuates LPS-Induced Inflammatory Response in Macrophages via NF-κB Signaling Pathway. *Mediators Inflamm.* **2019**, 3120391 (2019).

19. Zong, X. *et al.* Mettl3 Deficiency Sustains Long-Chain Fatty Acid Absorption through Suppressing Traf6-Dependent Inflammation Response. *J. Immunol. Author Choice* **202**, 567–578 (2019).

20. Wang, X. *et al.* The m6A Reader IGF2BP2 Regulates Macrophage Phenotypic Activation and Inflammatory Diseases by Stabilizing TSC1 and PPARγ. *Adv. Sci.* **8**, 2100209 (2021).

21. Cai, D., Sun, C., Murashita, T., Que, X. & Chen, S.-Y. ADAR1 non-editing function in macrophage activation and abdominal aortic aneurysm. *Circ. Res.* **132**, e78–e93 (2023).

22. Sun, C., Cai, D. & Chen, S.-Y. ADAR1 promotes systemic sclerosis via modulating classic macrophage activation. *Front. Immunol.* **13**, 1051254 (2022).

23. Medzhitov, R. & Horng, T. Transcriptional control of the inflammatory response. *Nat. Rev. Immunol.* **9**, 692–703 (2009).

24. Hargreaves, D. C., Horng, T. & Medzhitov, R. Control of Inducible Gene Expression by Signal-Dependent Transcriptional Elongation. *Cell* **138**, 129–145 (2009).

25. Mosser, D. M. & Edwards, J. P. Exploring the full spectrum of macrophage activation. *Nat. Rev. Immunol.* **8**, 958–969 (2008).

26. Serra, M., Forcales, S.-V., Pereira-Lopes, S., Lloberas, J. & Celada, A. Characterization of Trex1 Induction by IFN-γ in Murine Macrophages. *J. Immunol.* **186**, 2299–2308 (2011).

27. Yang, Y.-G., Lindahl, T. & Barnes, D. E. Trex1 Exonuclease Degrades ssDNA to Prevent Chronic Checkpoint Activation and Autoimmune Disease. *Cell* **131**, 873–886 (2007).

28. Bafica, A. *et al.* The IFN-Inducible GTPase LRG47 (Irgm1) Negatively Regulates TLR4-Triggered Proinflammatory Cytokine Production and Prevents Endotoxemia1. *J. Immunol.* **179**, 5514–5522 (2007).

29. Fee, B. E. *et al.* Type I interferon signaling and peroxisomal dysfunction contribute to enhanced inflammatory cytokine production in IRGM1-deficient macrophages. *J. Biol. Chem.* **300**, (2024).

30. Liu, Y. *et al.* Upregulation of Toll-Like Receptor 2 Gene Expression in Macrophage Response to Peptidoglycan and High Concentration of Lipopolysaccharide Is Involved in NF-κB Activation. *Infect. Immun.* **69**, 2788–2796 (2001).

31. Wang, T., Lafuse, W. P. & Zwilling, B. S. Regulation of Toll-Like Receptor 2 Expression by

Macrophages Following Mycobacterium avium Infection1. *J. Immunol.* **165**, 6308–6313 (2000).

32. Xiahou, Z. *et al.* NMI and IFP35 serve as proinflammatory DAMPs during cellular infection and injury. *Nat. Commun.* **8**, 950 (2017).

33. Fitzpatrick, J.-M. *et al.* MyD88-dependent and -independent signalling via TLR3 and TLR4 are differentially modulated by Δ9-tetrahydrocannabinol and cannabidiol in human macrophages. *J. Neuroimmunol.* **343**, 577217 (2020).

34. Latz, E. *et al.* TLR9 signals after translocating from the ER to CpG DNA in the lysosome. *Nat. Immunol.* **5**, 190–198 (2004).

35. Celhar, T. *et al.* TLR7 and TLR9 ligands regulate antigen presentation by macrophages. *Int. Immunol.* **28**, 223–232 (2016).

36. Boehm, U., Klamp, T., Groot, M. & Howard, J. C. Cellular responses to interferon-gamma. *Annu. Rev. Immunol.* **15**, 749–795 (1997).

37. Yeramian, A. *et al.* Arginine Transport via Cationic Amino Acid Transporter 2 Plays a Critical Regulatory Role in Classical or Alternative Activation of Macrophages1. *J. Immunol.* **176**, 5918–5924 (2006).

38. De Leon-Oliva, D. *et al.* AIF1: Function and Connection with Inflammatory Diseases. *Biology* **12**, 694 (2023).

39. Kim, Y.-H., Lee, J.-R. & Hahn, M.-J. Regulation of inflammatory gene expression in macrophages by epithelial-stromal interaction 1 (Epsti1). *Biochem. Biophys. Res. Commun.* **496**, 778–783 (2018).

40. Van Lint, P. & Libert, C. Matrix metalloproteinase-8: Cleavage can be decisive. *Cytokine Growth Factor Rev.* **17**, 217–223 (2006).

41. Nejati Moharrami, N., Bjørkøy Tande, E., Ryan, L., Espevik, T. & Boyartchuk, V. RORα controls inflammatory state of human macrophages. *PLoS ONE* **13**, e0207374 (2018).

42. Domanska, D. *et al.* Single-cell transcriptomic analysis of human colonic macrophages reveals niche-

specific subsets. *J. Exp. Med.* **219**, e20211846 (2022).

43. Ocaña-Guzman, R., Torre-Bouscoulet, L. & Sada-Ovalle, I. TIM-3 Regulates Distinct Functions in Macrophages. *Front. Immunol.* **7**, (2016).

44. Lee, B. *et al.* C/EBPα regulates macrophage activation and systemic metabolism. *Am. J. Physiol. - Endocrinol. Metab.* **306**, E1144–E1154 (2014).

45. Ramberg, V., Tracy, L. M., Samuelsson, M., Nilsson, L. N. & Iverfeldt, K. The CCAAT/enhancer binding protein (C/EBP) δ is differently regulated by fibrillar and oligomeric forms of the Alzheimer amyloid-β peptide. *J. Neuroinflammation* **8**, 34 (2011).

46. Patterson, J. B. & Samuel, C. E. Expression and regulation by interferon of a double-stranded-RNA-specific adenosine deaminase from human cells: evidence for two forms of the deaminase. *Mol. Cell. Biol.* **15**, 5376–5388 (1995).

47. Terajima, H. *et al.* N6-methyladenosine promotes induction of ADAR1-mediated A-to-I RNA editing to suppress aberrant antiviral innate immune responses. *PLOS Biol.* **19**, e3001292 (2021).

48. Bolger, A. M., Lohse, M. & Usadel, B. Trimmomatic: A flexible trimmer for Illumina sequence data. *Bioinformatics* **30**, 2114–2120 (2014).

49. Dobin, A. *et al.* STAR: Ultrafast universal RNA-seq aligner. *Bioinformatics* **29**, 15–21 (2013).

50. Li, H. *et al.* The Sequence Alignment/Map format and SAMtools. *Bioinformatics* **25**, 2078–2079 (2009).

51. Flati, T. *et al.* HPC-REDItools: a novel HPC-aware tool for improved large scale RNA-editing analysis. *BMC Bioinformatics* **21**, 353 (2020).

52. McLaren, W. *et al.* The Ensembl Variant Effect Predictor. *Genome Biol.* **17**, 122 (2016).

53. Feng, H., Conneely, K. N. & Wu, H. A Bayesian hierarchical model to detect differentially methylated loci from single nucleotide resolution sequencing data. *Nucleic Acids Res.* **42**, e69 (2014).

54. Patro, R., Duggal, G., Love, M. I., Irizarry, R. A. & Kingsford, C. Salmon provides fast and bias-aware

quantification of transcript expression. *Nat. Methods* **14**, 417–419 (2017).

55. Robinson, M. D., McCarthy, D. J. & Smyth, G. K. edgeR: a Bioconductor package for differential expression analysis of digital gene expression data. *Bioinforma. Oxf. Engl.* **26**, 139–40 (2010).

56. Soneson, C., Love, M. I. & Robinson, M. D. Differential analyses for RNA-seq: transcript-level estimates improve gene-level inferences. Preprint at https://doi.org/10.12688/f1000research.7563.1 (2016).

57. Lewis M., B. K., Rana S. EnhancedVolcano: Publication-ready volcano plots with enhanced colouring and labeling. (2024).

58. Yu, G., Wang, L.-G. & He, Q.-Y. ChIPseeker: an R/Bioconductor package for ChIP peak annotation, comparison and visualization. *Bioinforma. Oxf. Engl.* **31**, 2382–2383 (2015).

59. Zhang, F. & Chen, J. Y. HOMER: a human organ-specific molecular electronic repository. *BMC Bioinformatics* **12**, S4 (2011).